*Research Article*

Molecular Cancer Therapeutics

# Abrogation of *De novo* Lipogenesis by Stearoyl-CoA Desaturase 1 Inhibition Interferes with Oncogenic Signaling and Blocks Prostate Cancer Progression in Mice

Vanessa Fritz[1,2,3,4], Zohra Benfodda[1,2,3,4], Geneviève Rodier[5,6,7], Corinne Henriquet[1,2,3,4], François Iborra[8,9], Christophe Avancès[11,12], Yves Allory[13], Alexandre de la Taille[13], Stéphane Culine[13], Hubert Blancou[10], Jean Paul Cristol[8,9], Françoise Michel[8,9], Claude Sardet[5,6,7], and Lluis Fajas[1,2,3,4,8,9]

## Abstract

Increased *de novo* fatty acid (FA) synthesis is one hallmark of tumor cells, including prostate cancer. We present here our most recent results showing that lipid composition in human prostate cancer is characterized by an increased ratio of monounsaturated FA to saturated FA, compared with normal prostate, and evidence the overexpression of the lipogenic enzyme stearoyl-CoA desaturase 1 (SCD1) in human prostate cancer. As a new therapeutic strategy, we show that pharmacologic inhibition of SCD1 activity impairs lipid synthesis and results in decreased proliferation of both androgen-sensitive and androgen-resistant prostate cancer cells, abrogates the growth of prostate tumor xenografts in nude mice, and confers therapeutic benefit on animal survival. We show that these changes in lipid synthesis are translated into the inhibition of the AKT pathway and that the decrease in concentration of phosphatidylinositol-3,4,5-trisphosphate might at least partially mediate this effect. Inhibition of SCD1 also promotes the activation of AMP-activated kinase and glycogen synthase kinase 3$\alpha/\beta$, the latter on being consistent with a decrease in $\beta$-catenin activity and mRNA levels of various $\beta$-catenin growth-promoting transcriptional targets. Furthermore, we show that SCD1 activity is required for cell transformation by *Ras* oncogene. Together, our data support for the first time the concept of targeting the lipogenic enzyme SCD1 as a new promising therapeutic approach to block oncogenesis and prostate cancer progression. *Mol Cancer Ther; 9(6); 1740–54. ©2010 AACR.*

## Introduction

Prostate cancer is the most commonly diagnosed cancer and the second leading cause of cancer death in Western men after middle age and remained a major research and public health priority. Tumor growth is originally dependent on androgens, which exert their effects on prostate cancer cells by activating the androgen receptor, a member of the hormone nuclear receptor superfamily. In the mature prostatic gland, the androgen receptor regulates the expression of genes involved in diverse cellular functions, including survival and proliferation of the epithelial cells and lipid metabolism (1). In early-stage tumors, therapy based on androgen deprivation is only temporary effective (2), and many men develop recurrent androgen-independent prostate cancer, which has a very poor prognosis (3). In view of this, new therapeutic options are wanted.

One of the first identified biochemical hallmark of cancer cells was an alteration in metabolism. Early in the last century, Otto Warburg (1928) observed that tumors have a higher rate of glucose metabolism than normal tissues (4–6). Over the past decades, accumulating evidence of a metabolic reorganization has emerged from studies on various proliferating cells. Indeed, most tumor cells are characterized by higher rates of glycolysis, lactate production, and biosynthesis of lipids (7). Cells use two major sources of fatty acids (FA): exogenously derived (dietary) FA and *de novo* endogenously synthesized FA. *De novo* FA synthesis is very active during embryogenesis, whereas most adult normal cells and tissues, even those with high cellular turnover, preferentially use circulating FA for the synthesis of new structural

**Authors' Affiliations:** [1]Institut de Recherche en Cancérologie de Montpellier; [2]INSERM, U896; [3]Université de Montpellier 1; [4]CRLC Val d'Aurelle Paul Lamarque; [5]Institut de Génétique Moléculaire; [6]CNRS, UMR5535; [7]Université Montpellier 2; [8]Laboratoire de Biochimie, Centre Hospitalier Universitaire Lapeyronie; [9]UMR 204 Prévention des malnutritions et des pathologies associées, Institut Universitaire de Recherche Clinique; [10]Institut des Biomolécules Max Mousseron CNRS UMR5247 CC 1706, Université de Montpellier 2, Montpellier, France; [11]Service d'Urologie, CHU Groupe Hospitalisation Carémeau; [12]Service d'Urologie, Polyclinique Kennedy, Nîmes, France; and [13]CHU Henri Mondor, Creteil, France

**Note:** Supplementary material for this article is available at Molecular Cancer Therapeutics Online (http://mct.aacrjournals.org/).

V. Fritz and Z. Benfodda contributed equally to this work.

**Corresponding Author:** Lluis Fajas, Institut de Recherche en Cancérologie de Montpellier, CRLC Val d'Aurelle, Parc Euromédecine, F-34298, Montpellier Cedex 5, France. Phone: 33-4-67-61-24-28; Fax: 33-4-67-61-23-33. E-mail: lluis.fajas@inserm.fr

**doi:** 10.1158/1535-7163.MCT-09-1064

and signaling lipids. In contrast, it is now well documented that various tumors and their precursor lesions, including prostate cancer, undergo exacerbated endogenous FA biosynthesis irrespective of the levels of extracellular lipids (8, 9). The increased lipogenesis in cancer is reflected in overexpression and hyperactivity of lipogenic enzymes such as ATP citrate lyase, acetyl-CoA carboxylase, or the FA synthase (FAS; ref. 10). Moreover, studies with chemical inhibitors have revealed that inhibition of FAS activity results in decreased proliferation and increased apoptosis of cancer cells (11). *De novo* FA biosynthesis is required for cancer cells to synthesize new membranes, which have a particular lipidic composition that facilitates the formation of lipid rafts for increased signaling of cell growth receptors, such as erbB2 (12). Lipogenesis also participates in cancer cells to generate signaling molecules, such as phosphatidylinositol, phosphatidylserine, or phosphatidylcholine, which are important factors to activate proliferative and survival pathways. This is consistent with the observation that in most tumor cells examined, the majority of newly synthesized lipids are phospholipids (13, 14). We therefore hypothesized that targeting *de novo* lipid synthesis might abrogate tumor progression.

An important rate-limiting enzyme in lipogenesis is stearoyl-CoA desaturase 1 (SCD1), also commonly known as Δ9-desaturase. SCD1 is a microsomal enzyme that catalyzes the committed step in the biosynthesis of the monounsaturated FAs (MUFA) from saturated FAs (SFA) by introducing a *cis*-double bond to a fatty acyl-CoAs (15). The preferred substrates are palmitate (16:0) and stearate (18:0), which yield palmitoleate (16:1n-7) and oleate (18:1n-9), respectively. These represent the major MUFA of membrane phospholipids, triglycerides, wax esters, and cholesterol esters. Of note, most cancer cells contain higher levels of MUFA that tend to partition into detergent-resistant lipid rafts (reviewed in ref. 16). Because the ratio of MUFA to SFAs (desaturation index) affects phospholipid composition, and alteration in this ratio has been observed in several cancers (16), our main hypothesis in this study is that targeting SCD1 and associated lipid synthesis in prostate cancer cells might strongly affect their proliferation and/or survival, and represent a potent new therapeutic strategy to block prostate cancer progression.

As a proof of concept, we have characterized in this study the lipid composition and SCD1 expression in human prostate cancer tissue and analyzed the effects of SCD1 targeting in prostate cancer cells and prostate tumors in mice.

## Materials and Methods

### Chemicals

All solvents were high-performance liquid chromatography grade and were purchased from various suppliers. Methanol, chloroform, hexane, and isooctane were purchased from Carlo Erba. Potassium chloride and standards cholesterol esters, triacylglycerides, and phospholipids, and fatty methyl ester standards were purchased from Sigma-Aldrich. Phosphatidylinositol-3,4,5-trisphosphate [PI(3,4,5)$P_3$] was purchased from Cayman Chemical.

### BZ36 synthesis

6-[4-(2-Bromo-5-methoxy-benzoyl)-piperazin-1-yl]-*N*-phenylpropyl-nicotinamide compound was previously characterized as a specific competitive inhibitor of SCD1 with an $IC_{50}$ of 100 nmol/L (17). We have synthesized it in our laboratory as BZ36 compound according to the method described in the patent. Structure of the molecule is described in Supplementary Fig. S1.

### Human prostate tissue samples

Human prostate tissue was collected from consenting patients after protocol approval by the local ethics committee (CHU Henry Mondor, Creteil, France). Localized prostate cancer specimens from the peripheral zone of the prostate were obtained from men who had radical prostatectomy as treatment for their prostate cancer (Gleason $\geq$7; $n$ = 10). Nontumoral prostate specimens were obtained from men with benign hyperplasia of the prostate who had radical prostatectomy ($n$ = 10). The patients did not receive any hormonal or chemical treatment before obtaining tissue specimens. About the methods of tissue handling, the cancer specimens were examined on hematein-eosin–stained cryosections. As the cancer cells could be admixed with benign epithelial and stromal cells, areas with >70% of cancers cells were selected and macrodissected. For each selected area, 10 sections of 50-μm thickness (overall 10 mg tissue) were prepared and used for ratios of MUFA to SFA assessment, as well as for transcript analysis. For the benign prostatic hyperplasia specimens (including admixed benign epithelial and stromal cells), absence of malignant cells was verified on cryosections. The samples were then sectioned and processed as for the cancer specimens.

### Cell culture, transient transfections, and RNA interference experiments

The benign PNT2 prostate epithelial cell line was obtained from the European Collection of Animal Cell Cultures (Sigma-Aldrich). The androgen-sensitive LNCaP and the androgen-independent C4-2 human prostate carcinoma cell lines were purchased from Viromed Laboratory, Inc. Monolayer cell cultures were maintained in RPMI 1640 (Invitrogen) supplemented with 10% FCS, 100 units/mL penicillin, 100 μg/mL streptomycin, 10 mmol/L HEPES, and 1.0 mmol/L sodium pyruvate (Invitrogen) at 37°C in 5% $CO_2$. Primary mouse embryonic fibroblasts (MEF) were obtained from embryos at embryonic day 13.5 by standard methods. Monolayer cell cultures were grown in DMEM supplemented with 25 mmol/L glucose and 10% FCS. The transcriptional activity of the β-catenin–TCF4 complex was analyzed by doing transient transfections with 0.25 μg TCF/LEF-1

reporter (pTOP-FLASH) or control vector (pFOP-FLASH), which were kindly provided by Dr. Philippe Blache (Institut de Génomique Fonctionnelle, CNRS UMR5203, INSERM U661, Université Montpellier 1, Montpellier, France). Luciferase activities in cell lysates were normalized relative to the β-galactosidase activity to correct for differences in transfection efficiency. Figure shows representative results of at least two independent experiments done in triplicate. For small interfering RNA (siRNA) experiments, transfection of LNCaP or C4-2 cells was carried out with predesigned ON-TARGET plus siRNA oligonucleotide control or targeting the human SCD1 sequence GCACAUCAACUUCACCACA (Dharmacon). Nucleofection of cells with 2.5 μg siRNA was done on $2 \times 10^6$ cells using Amaxa Nucleofector R kit (Lonza). Twenty-four and 48 hours after transfection, cells were processed for cell proliferation by bromodeoxyuridine (BrdUrd) staining and harvested for RNA and protein analysis. For SCD1 overexpression experiments, nucleofection of LNCaP or C4-2 cells was done with 2 μg hSCD1 cDNA (Cliniscience) or control pcDNA3 (mock) vector using Amaxa Nucleofector R kit and cells were processed for cell proliferation by BrdUrd staining and harvested for RNA and protein analysis 72 hours after.

### Animal experiments

Male athymic nude mice (Foxn1 *nu/nu*; Harlan) were used at the age of 7 weeks (weight, 25–30 g). All procedures were done in compliance with the European Convention for the Protection of Vertebrate Animals Used for Experimentation (animal house agreement B-34-172-27, authorization for animal experimentation 34.324). Experiments were done at least twice for each tested condition. Animals were sacrificed before they became compromised. Xenografts were established by s.c. injecting $2 \times 10^6$ LNCaP cells, $2 \times 10^6$ C4-2 cells, or $5 \times 10^5$ HaRasV12-SV40 large T (Ras SV40)-transformed MEFs in 100 μL of a Matrigel solution. For curative experiments, tumors were allowed to grow until they were measurable with a caliper. In each group, the mice were randomized according to their established tumor volume and given SCD1 inhibitor BZ36 at 80 mg/kg in 100 μL of a Labrafil–DMA–Tween 80 solution (89:10:1; treated group) or vehicle alone (control group) by daily i.p. injection 5 days a week. For preventive experiments, the mice were treated daily for 7 days before the day of xenograft until the end of the experiment. Tumor volume measurements were taken two to tree times a week and calculated according to the following formula: length × width × height × 0.5236. Data are expressed as the mean tumor volume or as fold of the start point tumor volume. For survival analysis, animals bearing preestablished C4-2 tumors were treated with BZ36 at 80 or 160 mg/kg or with vehicle by daily i.p. injection 5 days a week. All mice were monitored for survival until tumor volume had reached 2,000 $mm^3$ or until death. Analysis of survival was conducted by a log-rank test based on the Kaplan-Meier method. At euthanasia, tumors were excised and either fixed in 4% formalin for immunohistologic analysis or prepared for FA analysis. Blood was harvested by cardiac puncture, and sera were prepared for further biochemical analysis.

### RNA isolation, reverse transcription, and quantitative real-time PCR

RNA was extracted with the use of TRI-Reagent (Euromedex) according to the manufacturers' recommendations. Reverse transcription of total RNA was done at 37°C using the Moloney murine leukemia virus reverse transcriptase (Invitrogen) and random hexanucleotide primers (Promega), followed by a 15-minute inactivation at 70°C. Quantitative PCR was conducted using the primers specific for human *SCD1* and SYBR Green LightCycler Master Mix (Eurofins MWG Operon). Measurement and analysis of gene expression were done using the ABI Prism 7300 Sequence detection System software (Applied Biosystems) under the following conditions: 2 minutes at 50°C and 10 minutes at 95°C, and then 40 cycles of 15 seconds at 95°C and 1 minute at 60°C. The relative content of cDNA samples was normalized by subtracting the threshold cycle ($C_t$) of the endogenous *18S* reference gene to the target gene ($\Delta C_t = C_t$ of target gene $- C_t$ of 18S). Values are expressed as the relative mRNA level of specific gene expression as obtained using the formula $2^{-(\Delta Ct)}$.

C4-2 cells treated with BZ36 at 25 μmol/L were analyzed for the expression profiles of 84 genes related to Wnt/β-catenin–mediated signal transduction by using Human Wnt Signaling Pathway PCR Array according to the manufacturers' recommendations (Tebu-Bio). The relative content of cDNA samples was normalized with the endogenous *β2M, HPRT1, RPL13*, and *GAPDH* reference genes, and the relative mRNA level was calculated according to the formula $2^{-(\Delta Ct)}$. Values are expressed as the fold change in relative mRNA level $[2^{-(\Delta Ct)}]$ following treatment of cells with BZ36 at 25 μmol/L compared with control.

### Proliferation assay

LNCaP, C4-2, PNT2, or MEFs cells were seeded in triplicate 24-well dishes at a density of $2.5 \times 10^4$ per well. At 24, 48, 72, and 96 hours following addition of increasing concentrations of BZ36 inhibitor of SCD1 in DMSO or DMSO alone, cells were trypsinized, pelleted by centrifugation at 1,200 rpm for 5 minutes, resuspended in 500 μL of culture medium, and counted in a hemocytometer. Figures show representative results of at least two independently done experiments.

### MTT assay

LNCaP, C4-2, or PNT2 cells were seeded in triplicate 24-well dishes at a density of $2.5 \times 10^4$ per well, and cell viability was tested after treatment with increasing concentrations of the BZ36 inhibitor of SCD1 for 48 hours. For rescue experiment, increasing concentrations of $PI(3,4,5)P_3$ from 1 to 20 μmol/L were added. After

48 hours, medium was removed and 250 μL of a 5 mg/mL MTT (Sigma) solution in PBS were added to each well. After 4 hours of incubation at 37°C, the MTT solution was removed, 200 μL DMSO (Sigma) was added, and cells were incubated for 5 minutes. Two hundred microliters of each sample were distributed in 96-well plates, and the reduction of yellow MTT to purple formazan product was measured by absorbance reading at 540 nm. Figures show representative results of at least two independently done experiments.

**Flow cytometry analysis of cell cycle and apoptosis**

For cell cycle analysis, LNCaP, C4-2, or PNT2 cells were plated at a density of $2.5 \times 10^5$ per well in six-well dishes and treated with increasing concentrations of the BZ36 inhibitor of SCD1 for 24 or 48 hours. Cells were then rinsed in PBS, pelleted at 400 × *g* for 5 minutes, and maintained on ice for 20 minutes before resuspension in a 25 μg/mL propidium iodide (Sigma) solution. Cells were kept overnight at 4°C, and the percentages of cells in $G_1$, S, and $G_2$-M phases of the cell cycle were measured with a Coulter Epics XL flow cytometer (Becton Dickinson) using 488-nm laser excitation. For apoptosis experiment, MEFs were treated with BZ36 at 25 μmol/L for 24 hours, then rinsed in PBS, pelleted at 400 × *g* for 5 minutes, and stained with Annexin V-FITC (Roche Diagnostics) for 15 minutes at 4°C. The percentage of Annexin V–positive cells was immediately analyzed using 488-nm laser excitation. Figures show representative results of at least two independently done experiments.

**Protein extracts and immunoblot analysis**

Protein extracts and SDS-PAGE, electrotransfer, and immunoblotting were done as previously described (18). The primary antibodies rabbit anti–AMP-activated kinase (AMPK), rabbit anti–phospho-AMPK ($Thr^{172}$), rabbit anti-AKT, and rabbit anti–phospho-AKT were purchased from Cell Signaling Technology. The primary antibody mouse anti–α-tubulin was purchased from Lab Vision (Thermo Fisher Scientific). The primary antibodies rabbit anti–p44/p42 mitogen-activated protein kinase (MAPK), rabbit anti–phospho-p44/p42 MAPK ($Thr^{202}/Tyr^{204}$), mouse anti–glycogen synthase kinase 3α/β (GSK3α/β), and rabbit anti–phospho-GSK3α/β were kindly provided by Dr. Gilles Freiss (Institut de Recherche en Cancérologie de Montpellier, INSERM U896, Université Montpellier 1, Montpellier, France). For phosphoproteome experiment, LNCaP and C4-2 cells treated with BZ36 at 25 μmol/L were analyzed for the relative phosphorylation of 46 kinase phosphorylation sites using human phospho-kinase array kit (Proteome Profiler) according to the manufacturers' recommendations (R&D Systems Europe). Level of phosphorylation was quantified using ImageJ software.

**FA analysis**

Total lipids from human prostate tissues were extracted thrice with 5 mL of Folch mixture [chloroform/methanol, 2:1 (v/v)] and 500 μL of water. Aliquots of the lipid extracts were dried under gaseous nitrogen, dissolved in 100 μL of the Folch mixture, and separated by TLC in different lipid subclasses (cholesterol ester, triacylglyceride, and phospholipid) using a hexane/ether/acetic acid (70:30:1, v/v) solvent system. To aid visualization, standards of cholesterol ester, triacylglyceride, and phospholipid were cospotted with samples. Spots were identified under UV light after spraying with 2′, 7′- dichlorofluorescein solution in ethanol and comparing with authentic standards. They were scrapped off the plates and converted to fatty methyl esters by transesterification with 3 mL of methanol/$H_2SO_4$ (19:1, v/v) at 90°C for 30 minutes. The different solutions were neutralized with 1 mL of aqueous solution of 10% of $K_2CO_3$, and fatty methyl esters were extracted with 5 mL of hexane. The fatty methyl esters were dried under gaseous nitrogen, subjected to gas chromatography (GC), and identified by comparison with standards (Sigma). Total lipids from liver tissues and C4-2 tumor xenografts from vehicle- or BZ36-treated animals were extracted thrice with Folch mixture, converted to fatty methyl esters as previously described, and subjected to GC identification. GC was conducted with a Thermo GC fitted with a flame ionization detector. A Supelcowax-10 fused silica capillary column (60 m × 0.32-mm inner diameter, 0.25-μm film thickness) was used, and oven temperature was programmed from 50°C to 200°C, increased 20°C per minute, held for 50 minutes, increased 10°C per minute to 220°C, and held for 30 minutes.

**Determination of SCD activity**

SCD activity was measured as previously described with some modifications (19). Briefly, subconfluent LNCaP, C4-2, and PNT2 of Ras SV40 MEFs cells grown in six-well plate were incubated with BZ36 at 25 μmol/L for 2 hours in serum and FA-free DMEM supplemented with 0.2% bovine serum albumin (BSA). In this environment, the cells are solely dependent on endogenous FA synthesis for production of storage, structural, and signaling lipids. Trace amount of [$^{14}$C]palmitic acid was then added to the culture (0.5 μCi/well), and cells were incubated for 6 more hours. At the end of the incubation, total cell lipids were extracted and saponified, and then released FAs were esterified with boron trifluoride in methanol for 90 minutes at 100°C. The derived methyl esters were separated by argentation TLC (Thermo Fisher Scientific) following the procedure of Wilson and Sargent (20) using a solvent phase consisting of hexane/ethyl ether (90:10, v/v). Pure stearic and oleic methyl ester acids were run in parallel to the samples. Air-dried plates were scanned on a PhosphorImager, and FA spots on TLC were analyzed with PhosphorImager software. SCD activity was expressed as the ratio of palmitoleic on palmitic methyl ester acids and normalized to cellular DNA content.

### Measurement of *de novo* FA synthesis

The inhibitor BZ36 was added overnight at a final concentration of 25 μmol/L to subconfluent cultures of cells grown in six-well plate in serum and FA-free DMEM supplemented with 0.2% BSA. Cultures were then labeled in triplicate with 1.0 μCi of [$^{14}$C]palmitate or [$^{14}$C]stearate for 6 hours, and total lipids were Folch extracted with chloroform/methanol. Labeled lipids were subjected to TLC in hexane/diethyl ether/acetic acid (90:10:1, v/v) to separate cholesterol ester, triglycerides, and phospholipids. Standards were run for each of the lipid classes. After chromatography, labeled lipid classes were quantified by scintillation counting and radioactivity was normalized to DNA content.

### PI(3,4,5)$P_3$ measurement

The production of PI(3,4,5)$P_3$ in LNCaP and C4-2 prostate cancer cells was measured 24 hours following exposure to control medium or to medium supplemented with BZ36 at 25 μmol/L. The levels of produced PI(3,4,5)$P_3$ were quantified after cellular lipid extraction using a PI(3,4,5)$P_3$ mass ELISA kit according to the manufacturer's instruction.

### Immunofluorescence and immunohistochemistry of hSCD1

Immunohistochemical analysis of SCD1 expression was done using high-density tissue microarray slide (Accumax array) with 39 prostate adenocarcinoma spots from different patients (Gleason scores from 5 to 9) with corresponding normal tissues. Immunohistochemical analysis of proliferating cell nuclear antigen (PCNA) expression was done on 5-μm paraffin-embedded sections of LNCaP, C4-2, or Ras SV40 Large T-transformed–MEF tumor xenografts. Briefly, after antigen retrieval, deparaffinized sections were blocked with Fc receptors with PBS containing 5% goat serum and then incubated with corresponding anti-SCD1 mouse antibody (1:50; Abcam) or anti-PCNA mouse antibody (1:50; Santa Cruz Biotechnology) in PBS–0.1% Tween overnight at 4°C. SCD1 staining was revealed with a peroxidase-conjugated anti-mouse secondary antibody (1:100; Jackson Immuno Research) and the 3,3′-diaminobenzidine chromogen (Dako) as substrate. Sections were counterstained with Mayer's hematoxylin. PCNA staining was revealed by immunofluorescence using a FITC-conjugated anti-mouse secondary antibody (1:150; Jackson ImmunoResearch). Sections were mounted in Mowiol and analyzed rapidly.

### Immunocytochemistry

Immunocytochemical analysis of SCD1 expression was done on PNT2, LNCaP, and C4-2 cells grown on coverslip. Briefly, after fixation in 4% paraformaldehyde and permeabilization with 0.5% Triton X-100, cells were incubated with blocking buffer (PBS–1% BSA). SCD1 staining was detected with an anti-SCD1 mouse primary antibody (1:50; Abcam) for 1 hour at 37°C and revealed with a FITC-conjugated anti-mouse secondary antibody (1:150; Jackson ImmunoResearch) for 30 minutes at 37°C. Slides were mounted in Mowiol and analyzed rapidly.

### BrdUrd staining

LNCaP and C4-2 cells grown on coverslips were incubated for 4 hours with BrdUrd (100 μmol/L final) at 24 and 48 hours following SCD1 knockdown. Cells were then fixed and permeabilized with cold methanol for 10 minutes at −20°C. After three washes with PBS, DNA was denaturized with 4 N HCl for 10 minutes at room temperature, and cells were incubated with blocking buffer (PBS–1% BSA). BrdUrd was then detected with anti-BrdUrd monoclonal antibody (1:50; Dako) for 1 hour at 37°C. After three washes with PBS, cells were incubated with a FITC-conjugated anti-mouse secondary antibody (1:150; Jackson ImmunoResearch) for 30 minutes at 37°C, and slides were mounted in Mowiol.

### Statistical analysis

Statistical analysis was done with unpaired Student's *t* test. Differences were considered statistically significant at $P < 0.05$ (*, $P < 0.05$; **, $P < 0.01$; ***, $P < 0.001$). The log-rank test was used to assess the statistical significance of differences in animal survival along the treatment groups.

## Results

### MUFA content and SCD1 expression are increased during prostate cancer progression

As a first approach to target lipid synthesis pathways in cancer cells, we measured FA composition during prostate cancer progression. The ratio of total MUFA to SFA was significantly increased in cholesterol ester, triacylglyceride, and phospholipid lipid fractions in human prostate cancer tissue samples with Gleason score of ≥7 (Fig. 1A), suggesting the participation of desaturase enzymes. Interestingly, among the analyzed MUFAs, those produced by a Δ9-desaturase activity, in majority palmitoleate (16:1n-7) and oleate (18:1n-9), were the most abundant in all lipid subclasses (data not shown). Furthermore, the specific desaturation indexes 16:1n-7/16:0 (Fig. 1B) and 18:1n-9/18:0 (Fig. 1C) were increased in human prostate samples, supporting the participation of the Δ9-desaturase enzyme. Consistent with this observation, SCD1 was increased in cancerous, compared with normal human prostates at both mRNA (Fig. 1D) and protein (Fig. 1E) levels, as analyzed by quantitative PCR and immunohistochemical studies, respectively. SCD1 expression was also increased, as measured by immunofluorescence in the human prostate cancer cell lines LNCaP and C4-2, compared with the nontumoral PNT2 benign prostate cell line (Fig. 1F).

### Pharmacologic and genetic inhibition of SCD1 activity induces growth arrest of prostate cancer cell lines *in vitro*

Because MUFA synthesis and SCD1 expression are both increased in prostate cancer, we next evaluated the effects of inhibition of SCD1 activity, measured by the conversion of exogenous $^{14}$C-saturated palmitic acid (16:0) substrate to monounsaturated palmitoleic acid (16:1n-7), on lipid synthesis and proliferation in prostate cancer cell lines. In a pharmacologic approach, one of the first small-molecule SCD1 inhibitors, the 6-[4-(2-bromo-5-methoxy-benzoyl)-piperazin-1-yl]-*N*-phenyl-propyl-nicotinamide compound (17) was synthesized as BZ36 and used in this study (Supplementary Fig. S1). BZ36 compound has been characterized to specifically inhibit the biological activity of stearoyl-CoA Δ-9 desaturase but not Δ-5 desaturase, Δ-6 desaturase, or FAS. In all three cell lines tested, a marked reduction of the labeled monounsaturated palmitoleic acid was observed in BZ36-treated compared with control cells (Fig. 2A–D). Interestingly, basal SCD1 activity was progressively increased from nontumoral PNT2 to androgen-independent C4-2 cell lines (Fig. 2D), further suggesting the implication of SCD1 in prostate cancer progression. Inhibition of SCD1 activity with BZ36 correlated with a dose-dependent decrease in cell proliferation of LNCaP, and C4-2 cancer cells, reaching 100% inhibition at the maximal dose used (Fig. 2E and F). Flow cytometry analysis further showed the inhibitory effects of BZ36 in prostate cancer cells, showing accumulation of cells in the $G_0$-$G_1$ phase of the cell cycle, concomitant with a decrease in the S phase (Supplementary Fig. S2). Strikingly, no effect in proliferation was observed in the noncancerous PNT2 cell line even at a maximal dose (Fig. 2G). Similar to what was observed using SCD1 small-molecule inhibitors, genetic SCD1 inhibition using siRNA technology blocked SCD1 protein expression (Fig. 2H; Supplementary Fig. S3) and resulted in a marked decrease in proliferation in both LNCaP and C4-2 cell types (Fig. 2I and J).

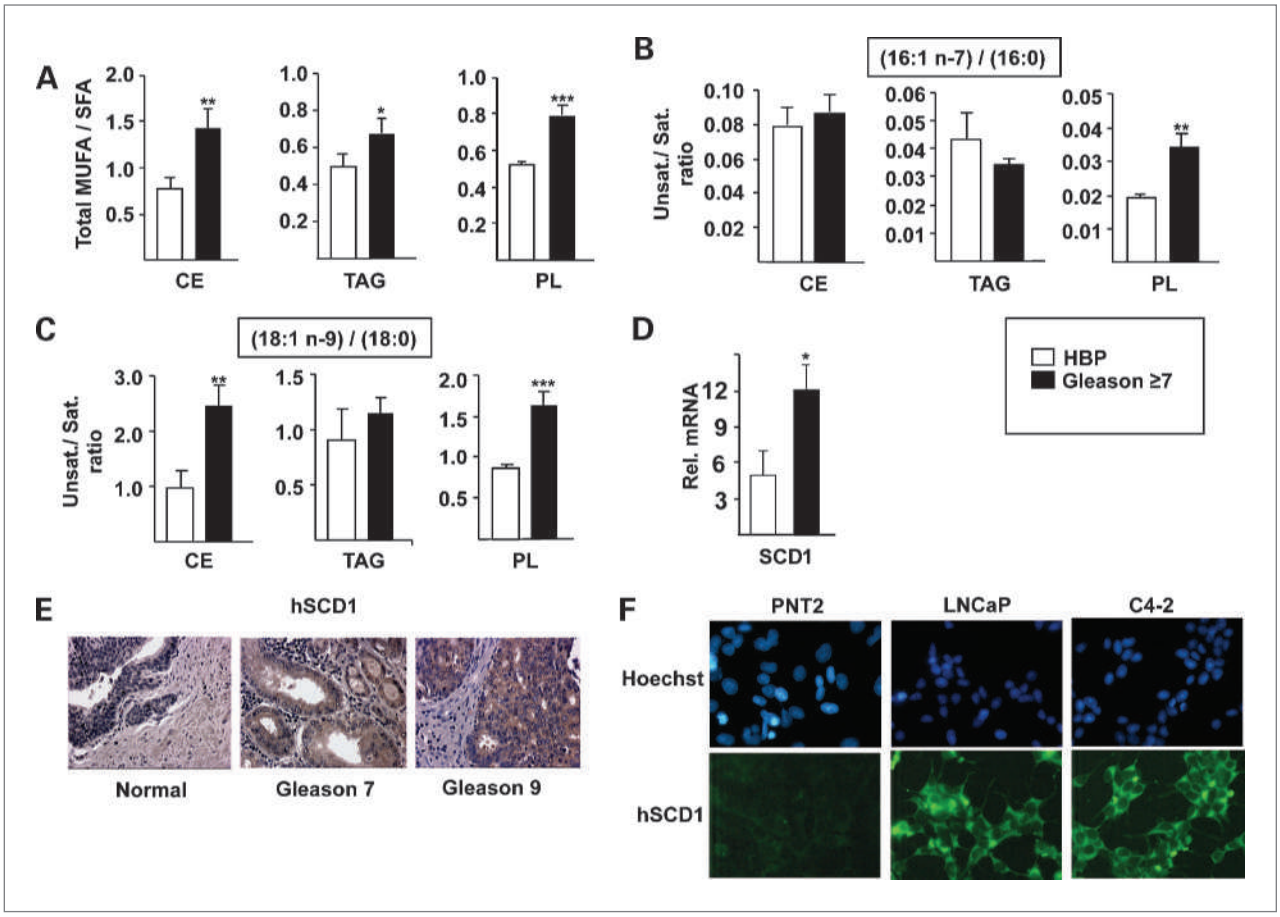


Figure 1. MUFA content and SCD1 expression are increased with prostate cancer progression. The global desaturation index, which corresponds to the ratio of total MUFA to SFAs (A), and the specific desaturation indexes 16:1n-7/16:0 (B) and 18:1n-9/18:0 (C) in cholesterol esters (CE), triacylglycerides (TAG), and phospholipids (PL) are increased in prostate cancer tissue with Gleason score ≥7. Columns, mean; bars, SD. Human SCD1 is overexpressed in prostate cancer tissue with Gleason score ≥7 at mRNA (D) and protein (E) levels. F, the level of SCD1 expression was compared by immunofluorescence in PNT2 benign prostate cell line and in LNCaP and C4-2 tumoral prostate cell lines. *, $P < 0.05$; **, $P < 0.01$; ***, $P < 0.001$.

These results suggested that, first, SCD1 activity and lipid synthesis are required in prostate cancer cells to proliferate. Second, noncancer cells do not require *de novo* lipid synthesis, and therefore, normal cells are not sensitive to inhibition of this pathway. Third, the inhibitory effects of SCD1 inhibitors are mediated by SCD1 because the same effects are observed when SCD1 is depleted from the cells.

To further document the relation between the level of SCD1 expression and the proliferative potential of prostate cancer cells, we analyzed the effect of overexpressing SCD1 in cells. We show that SCD1 overexpression in LNCaP and C4-2 cells was associated to a 13.7% and 20.5% increase in proliferation, respectively, as assessed by measuring the percentage of BrdUrd-incorporating proliferative cells at 72 hours following transient transfection with SCD1 cDNA compared with mock transfection (Supplementary Fig. S4). This rather modest increase in proliferation indicates that endogenous SCD1 expression levels are likely sufficient to drive changes in lipid synthesis required for proliferation of cancer cells.

### Inhibition of SCD1 activity decreases *de novo* FA synthesis in prostate cancer cell lines

The effects of SCD1 in cell proliferation were likely mediated by the participation of this enzyme in the *de novo* FA synthesis pathways. This was consistent with the observation that [$^{14}$C]palmitate incorporation into cholesterol ester, triacylglyceride, and phospholipid, which is a measure of *de novo* lipid synthesis, was inhibited by 39%, 27%, and 58%, respectively, in LNCaP cells (Fig. 3A) and by 33%, 24%, and 41%, respectively, in C4-2 cells (Fig. 3B) treated with BZ36. Similarly, [$^{14}$C]stearate incorporation into cholesterol ester, triacylglyceride, and phospholipid was also inhibited by 77%, 78%, and 81%, respectively, in LNCaP cells (Fig. 3D) and by 70%, 19%,

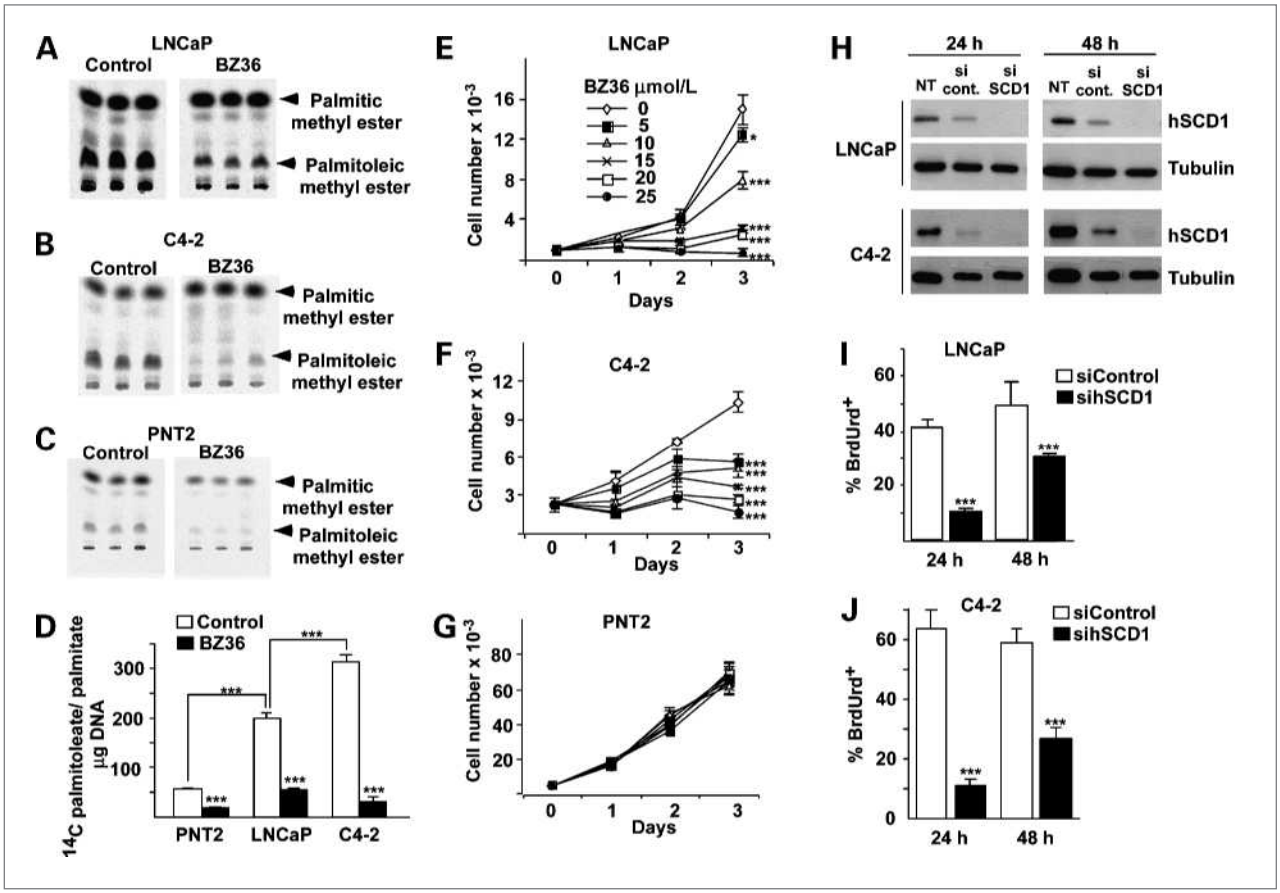


Figure 2. Inhibition of SCD1 activity induces growth arrest of prostate cancer cells *in vitro*. A to D, autoradiography of TLC showing quantification of SCD1 Δ9-desaturase activity on LNCaP (A), C4-2 (B), and PNT2 (C) cells by measuring the conversion of exogenous $^{14}$C-saturated palmitic acid substrate into monounsaturated palmitoleic acid in control or 25 µmol/L BZ36–treated cells. D, SCD1 desaturase activity was expressed as the ratio of palmitoleic acid to palmitic acid after normalization to cellular DNA content. E to G, proliferation of tumoral LNCaP (E), C4-2 (F), and benign PNT2 (G) cells was measured with a hematocytometer at 24, 48, and 72 h following culture with increasing doses of BZ36. H, SCD1 immunoblot in LNCaP and C4-2 cell lines 24 and 48 h after transfection with control or siRNA against hSCD1. I and J, proliferation of LNCaP (I) and C4-2 (J) cells was measured by counting the percentage of BrdUrd incorporation at 24 and 48 h after siRNA transfection. Columns, mean of at least two independent experiments done in triplicates; bars, SD. *, $P < 0.05$; ***, $P < 0.001$.

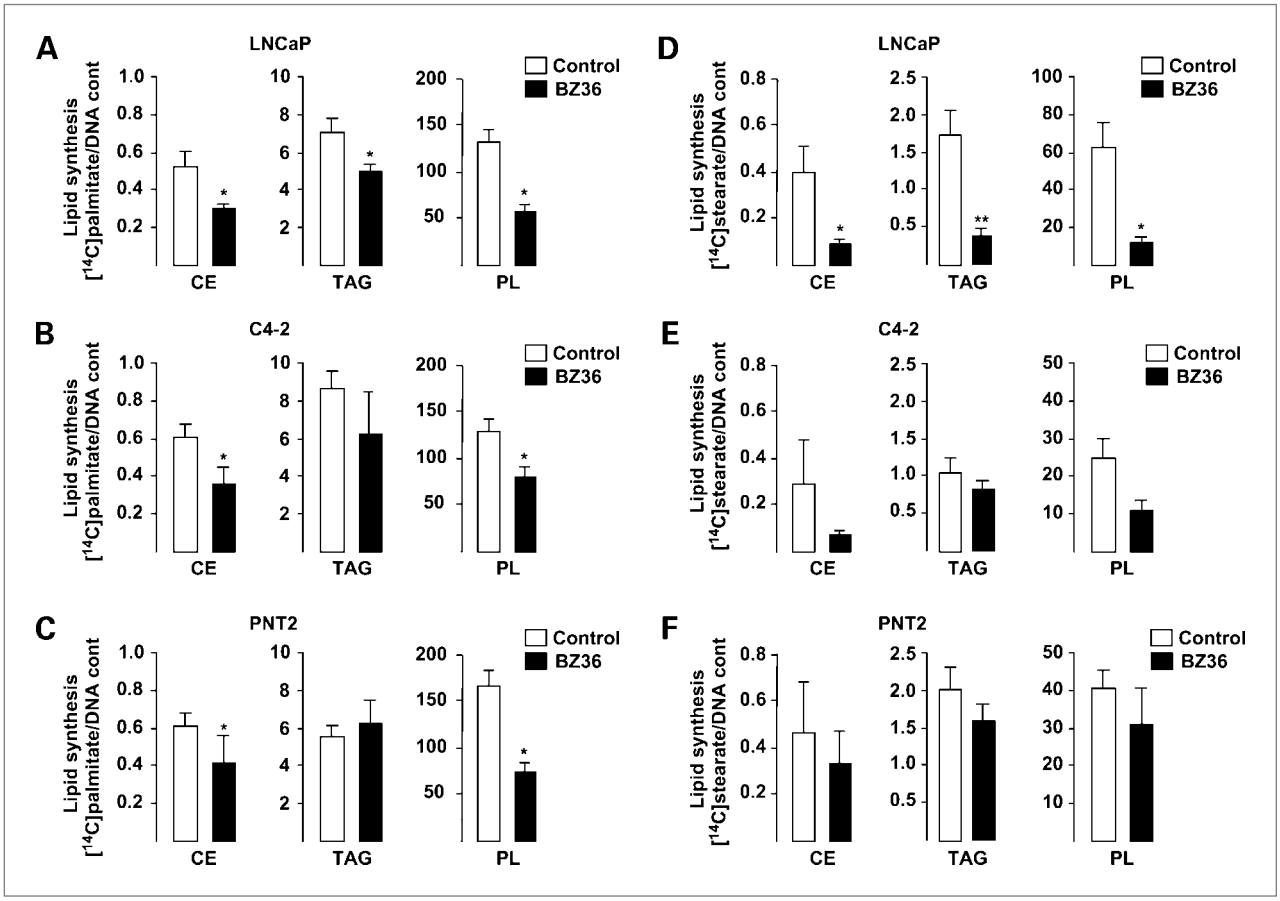


Figure 3. Inhibition of SCD1 activity abrogates *de novo* FA synthesis in prostate cancer cells *in vitro*. A to C, [$^{14}$C]palmitate incorporation into cholesterol ester, triacylglyceride, and phospholipid was measured in LNCaP (A), C4-2 (B), and PNT2 (C) cells after exposure to control media or 25 μmol/L BZ36. D to F, [$^{14}$C]stearate incorporation into cholesterol ester, triacylglyceride, and phospholipid was measured in LNCaP (D), C4-2 (E), and PNT2 (F) cells after exposure to control medium or 25 μmol/L BZ36 inhibitor. Columns, mean of at least two independent experiments done in triplicates; bars, SD. *, $P < 0.05$; **, $P < 0.01$.

and 49%, respectively, in C4-2 cells (Fig. 3E) treated with BZ36. Similar results were observed in PNT2 cells (Fig. 3C and F).

## SCD1 inhibition interferes with major signaling pathways in prostate cancer cells

Lipids are important signaling molecules that actively participate in triggering specific phosphorylation pathways. Because inhibition of SCD1 activity was associated with a significant reduction in *de novo* lipid synthesis in prostate cancer cells (Fig. 3), we expected also a decrease in these pathways. The relative phosphorylation status of several kinases in both LNCaP and C4-2 cells in response to treatment with BZ36 showed similar important changes compared with control (Fig. 4A and B; Supplementary Fig. S5). Relevant for our study was the decrease in AKT phosphorylation (S473/T308) levels in BZ36-treated LNCaP (Fig. 4A) and C4-2 (Fig. 4B) compared with nontreated cells. Significant decreases were also observed in the phosphorylation levels of extracellular signal-regulated kinase (ERK) 1/2 (T202/Y204, T185/Y187) and MAPK/ERK kinase 1/2 (S218/S222, S222/S226) in BZ36-treated C4-2 cells compared with control cells. Interestingly, phosphorylation of AMPKα (T174) was increased following BZ36 treatment in both LNCaP and C4-2 cancer cells (Fig. 4A and B). Western blot analysis further proved phosphorylation changes in these proteins (Fig. 4C and D). Inhibition of AKT phosphorylation was not the result of decreased expression of AKT because total AKT protein levels were similar in treated and not treated cells (Fig. 4C). In contrast to AKT, BZ36 treatment induced a significant increase in phosphorylated AMPKα in both LNCaP and C4-2 cells (Fig. 4C). Interestingly, BZ36 activated AMPK more efficiently than the classic AMPK activator AICAR (Fig. 4C). We next investigated the active phosphorylation status of downstream signaling proteins, such as ERK1/2. Immunoblot analysis revealed decreased phosphorylation of ERK1/2 in both LNCaP and C4-2 cells following exposure to BZ36, whereas total ERK expression was not changed (Fig. 4D). Moreover, we found that phosphorylation of GSK3α/β

(S21/S9), which is inhibited by phosphorylation by AKT, was also abrogated by BZ36 treatment in LNCaP and C4-2 cells (Fig. 4D). These results were consistent with the abrogation of at least AKT signaling in BZ36-treated cells.

AKT is activated by PI(3,4,5)$P_3$, which is the result of PIP2 phosphorylation by phosphatidylinositol 3-kinase. Because SCD1 inhibition induced a dramatic decrease in *de novo* synthesis of phospholipids, which are PI(3,4,5)$P_3$ precursors, we anticipated that BZ36 would have an effect in PI(3,4,5)$P_3$ concentration in these prostate cancer cells. ELISA test showed that PI(3,4,5)$P_3$ concentration was strongly decreased by 84% and 92%, respectively, in LNCaP and C4-2 BZ36-treated compared with

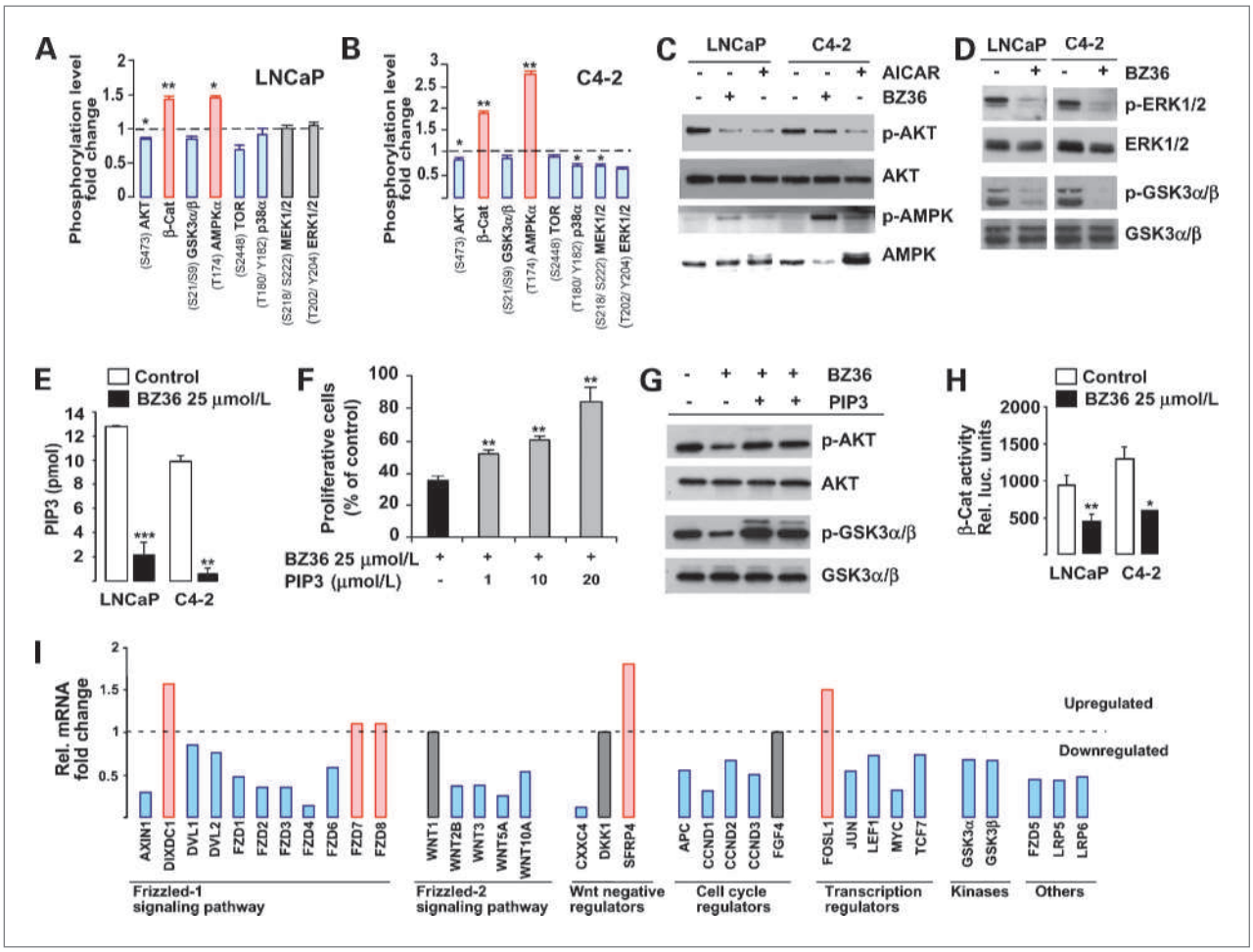


Figure 4. Inhibition of SCD1 activity decreases AKT/PI(3,4,5)$P_3$ and GSK3α/β/β-catenin signaling pathways in prostate cancer cells *in vitro*. A and B, proteome analysis of the change in the phosphorylation status of indicated kinases in LNCaP (A) and C4-2 (B) cells 24 h after culture with 25 μmol/L BZ36 inhibitor. Level of phosphorylation was quantified using ImageJ software. Values are represented as relative fold change of phosphorylation level in cells treated with 25 μmol/L BZ36 inhibitor compared with cells cultured in control medium. Increase and decrease in phosphorylation level are indicated in red and blue, respectively. Columns, mean; bars, SD. MEK, MAPK/ERK kinase. C, immunoblot analysis of phospho-AKT, total AKT, phospho-AMPK, and total AMPK in LNCaP and C4-2 cells at 24 h following exposure to control media, 25 μmol/L BZ36 inhibitor, or 1 mmol/L AICAR. D, immunoblot analysis of phospho-ERK1/2, total ERK1/2, phospho-GSK3α/β, and total GSK3α/β in LNCaP and C4-2 cells at 24 h following exposure to control media or 25 μmol/L BZ36 inhibitor. E, the levels of PI(3,4,5)$P_3$ produced were measured by ELISA on lipid extracts from LNCaP and C4-2 cells 24 h following treatment with BZ36 at 25 μmol/L or with control medium. Data are expressed in pmol. Columns, mean; bars, SD. F, rescue of BZ36-treated C4-2 cell proliferation by increasing PI(3,4,5)$P_3$ amounts was measured by MTT assay. Forty-eight hours after treatment, the enzymatic reduction of MTT to formazan was quantified by absorbance reading at 540 nm. Columns, mean; bars, SD. G, rescue of BZ36-treated C4-2 cell signaling by increasing PI(3,4,5)$P_3$ amounts was evaluated by immunoblot analysis of phospho-AKT, total AKT, phospho-GSK3α/β, and total GSK3α/β 24 h following exposure to 25 μmol/L BZ36 inhibitor. H, measurement of β-catenin luciferase reporter activity in LNCaP and C4-2 cells 24 h after exposure to control media or 25 μmol/L BZ36 inhibitor. Columns, mean; bars, SD. I, analysis of mRNA expression level variation of genes related to the Wnt/β-catenin signaling pathway in C4-2 cells 24 h following exposure to 25 μmol/L BZ36 inhibitor. Genes are grouped according to their belonging to cell surface receptors (members of the Frizzled-1 signaling pathway), glycosylated extracellular signaling molecules (members of the Frizzled-2 signaling pathway), Wnt binding antagonists and regulators of cell cycle, and proliferation and transcription relative to the Wnt signaling pathway. Genes that are upregulated are indicated in red and genes that are downregulated are indicated in blue. Data are representative of at least two independent experiments. *, $P < 0.05$; **, $P < 0.01$; ***, $P < 0.001$.

nontreated cells (Fig. 4E). These results suggested that inhibition of AKT activity in these cells was mediated, at least partially, by decreased synthesis of PI(3,4,5)$P_3$ precursors after BZ36 treatment. To further document the implication of PI(3,4,5)$P_3$ in mediating SCD1 effect, we asked whether addition of external PI(3,4,5)$P_3$ could rescue cells from the effect of SCD1 inhibition on cell proliferation and signaling. As shown in Fig. 4F, the percentage of proliferative C4-2 cells 48 hours following treatment with 25 μmol/L of SCD1 inhibitor BZ36 was only 35% that of untreated control cells. In contrast, addition of increasing doses of PI(3,4,5)$P_3$ at 1, 5, or 10 μmol/L in the presence of 25 μmol/L BZ36 significantly rescued cell proliferation in a dose-dependent manner at 52%, 61%, and 84% of control, respectively (Fig. 4F). The increase in cell proliferation following PI(3,4,5)$P_3$ treatment in the presence of BZ36 was correlated with an increase of the AKT activity, as measured by an increase of the phosphorylated AKT (S473/T308) and GSKα/β proteins (Fig. 4G). Increase of phosphorylation was not the result of increased expression of AKT and GSKα/β because total AKT and GSKα/β protein levels were similar in treated and not treated cells.

It was also particularly interesting the effects on GSK3α/β, which is further downstream AKT pathway (Fig. 4G-H). Activation of GSK3α/β by SCD1 inhibitors resulted in the disruption of β-catenin signaling, shown by the decreased activity of a β-catenin reporter in response to BZ36 in both LNCaP and C4-2 cells (Fig. 4H). This was fully consistent with changes in the expression of genes in the β-catenin pathway, including, but not limited to, decreased expression of several members of the frizzled family; decreased *cyclin D1, cyclin D2, cyclin D3, myc,* or *c-jun* expression; or decreased expression of several *Wnt* family members in C4-2 cells treated with BZ36 (Fig. 4I). Taken together, these results proved that SCD1 inhibition directly or indirectly results in a strong disruption of major signaling pathways implicated in cell proliferation, migration, and survival.

### Inhibition of SCD1 activity inhibits LNCaP and C4-2 tumor growth *in vivo*

We next evaluated whether reduction of SCD1 activity by BZ36 could inhibit the growth of preestablished prostate cancer tumors in mice, a clinically relevant situation. LNCaP and C4-2 cells were injected s.c. in male athymic nude mice. Treatment of each individual mouse started when tumor nodules were measurable. In two independent experiments, we observed that treatment of mice with 80 mg/kg BZ36 5 days a week during 21 days signi ficantly inhibited both androgen-dependent LNCaP (Fig. 5A and B) and androgen-insensitive C4-2 (Fig. 5D and E) tumor volume and tumor growth rate compared with control mice that received vehicle only. Moreover, we observed that BZ36 treatment at 80 mg/kg induced LNCaP and C4-2 tumor regression in 27% of LNCaP (Fig. 5B) and 19% of C4-2 (Fig. 5E) xenografted mice, whereas no tumor regression was observed in control mice. On the opposite, we observed that LNCaP or C4-2 tumor volume was increased >4-fold in 42% of vehicle-treated mice, whereas this was the case in only 18% (LNCaP) and 12% (C4-2) of BZ36-treated mice (Fig. 5B and E). Immunostaining of tumors from LNCaP (Fig. 5C) and C4-2 (Fig. 5F) xenografts for the proliferation-associated marker PCNA confirmed the effect of BZ36 on tumor cell proliferation with an average 50% decrease of PCNA-positive cells in tumors from animals treated with BZ36 at 80 mg/kg compared with tumors from control animals. We next investigated whether the reduction of tumor growth following SCD1 inhibition was associated to changes in FA composition *in vivo*. Analysis of total lipids extracted from both liver and tumor tissues revealed that the specific ratios of 16:1n-7/16:0 and 18:1n-9/18:0 FA were significantly reduced in both tissues in mice receiving BZ36 treatment compared with control mice (Fig. 5G). This indicates that the observed effects of BZ36 treatment on tumor growth are specific to inhibition of SCD1 Δ9-desaturase activity.

We next examined whether BZ36 treatment improved the survival of mice with preestablished androgen-independent prostate cancer tumors derived from C4-2 cells. Nude mice were treated with vehicle or two doses of BZ36, 80 or 160 mg/kg, and followed until death or until tumor volume reached 2,000 $mm^3$. Among mice bearing subcutaneous C4-2 tumors, BZ36 treatment of animals results in significant and dose-dependant prolongation of animal survival in comparison with vehicle control ($P = 0.038$; Supplementary Fig. S6). Indeed, after the treatment was started, the median survival in the control group was 14 days, although it was 21 days in animals treated with 80 mg/kg BZ36. At 14 days of treatment, 37.5% of animals survived in the control group against 75% and 100% in the groups treated with 80 mg/kg BZ36 and 160 mg/kg BZ36, respectively. At 28 days of treatment, 75% of animals receiving 160 mg/kg BZ36 survived against only 12.5% in the control group.

Importantly, no significant weight loss or other toxicity was observed in mice following daily i.p. injection of BZ36 compound (Supplementary Fig. S7A–C). Histologic examination confirmed the absence of toxicity in liver and skin and no difference of tissue integrity between control and BZ36-treated animals (Supplementary Fig. S7D). Moreover, biochemical analysis of mice sera confirmed the absence of toxicity in liver and kidney. Liver function, assessed by measurement of albumin and bilirubin levels, as well as the enzymes alkaline phosphatase, alanine aminotransferase, and aspartate aminotransferase activities, was similar between control and BZ36-treated animals. Creatinine and urea blood levels were also similar between control and BZ36-treated animals, revealing an intact kidney metabolism (Supplementary Fig. S7E).

### Inhibition of SCD-like activities results in p53-independent loss of viability and reduces tumorigenicity of transformed MEFs

To further document the strong antiproliferative effects of SCD inhibitors on Ras-transformed cells, we next tested their effect on MEFs transformed by genetically defined elements or genetic background that cooperate with Ras in transformation. Proliferation index of MEFs fully transformed by activated Ras (HaRasV12) and SV40 large T was strongly decreased by BZ36 treatment (Fig. 6A), whereas that of the slowly growing normal MEFs (wild-type) was only moderately reduced. Similar to prostate cancer cells, inhibition of SCD activity in these transformed MEFs resulted in decreased lipogenesis as measured by the decrease of [$^{14}$C] palmitoleic acid to [$^{14}$C]palmitic methyl ester acid ratio (Fig. 6B).

Importantly, the potent antiproliferative effect of BZ36 on cells containing large T confirmed that SCD inhibition has effect on cells with altered pRB and p53 pathways, a hallmark of most cancer cells. Consistently, BZ36 also efficiently blocked the proliferation of p53$^{-/-}$ MEFs fully transformed by HaRasV12 (Fig. 6C). Interestingly, these antiproliferative effects of BZ36 were associated with a strong induction of cell death (Annexin V–positive cells) in all transformed cells, including p53$^{-/-}$ MEFs transformed by activated Ras, suggesting that the end result of SCD inhibition in cancer cells is a p53-independent cell death (Fig. 6D).

To further investigate the effects of BZ36 on transformed MEFs, we next tested its effect on the capacity of these cells to form tumors when injected in nude mice. Two days after their injection with HaRasV12-SV40 large T–transformed MEFs, mice were treated with BZ36 or

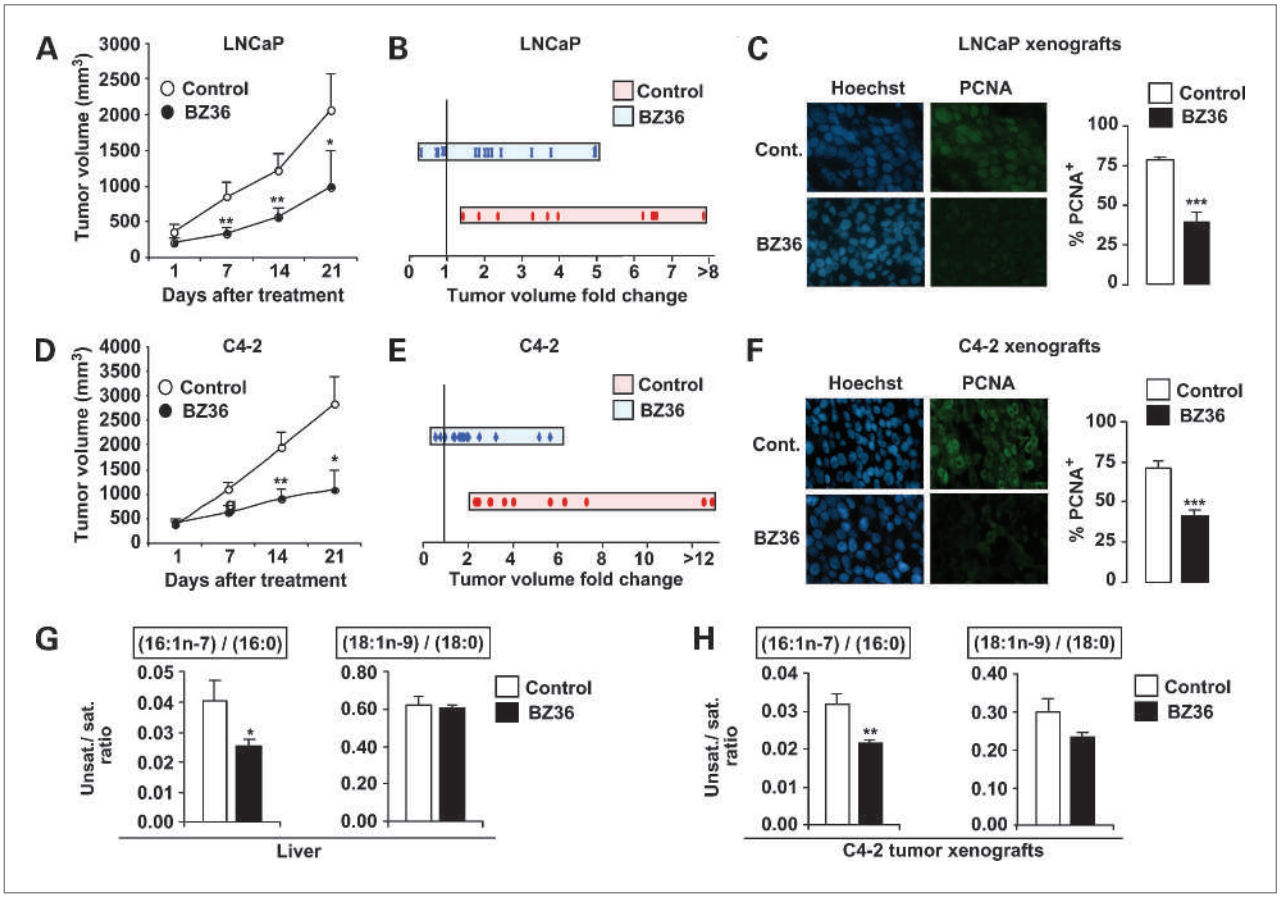


Figure 5. Inhibition of SCD1 activity decreases tumor growth of prostate cancer xenografts *in vivo*. Tumor volume progression of s.c. implanted LNCaP (A and B) or C4-2 (D and E) cells in nude athymic mice was measured weekly following daily i.p. injection with BZ36 at 80 mg/kg or with vehicle. A and D, points, mean tumor volume (mm$^3$) from day 1 to day 21; bars, SE. B and E, values are expressed as the fold change to initial tumor volume (day 14/day 1). Quantification of PCNA immunostaining of proliferative LNCaP (C) and C4-2 (F) cells s.c. implanted 14 d following daily i.p. injection with BZ36 at 80 mg/kg or with vehicle. Six fields per section were analyzed for PCNA immunostaining indicative of cell proliferation. Sections of tumors of all mice were analyzed. At least 300 cells were counted per tumor. Data are representative of at least three independent experiments. G and H, the specific desaturation indexes 16:1n-7/16:0 and 18:1n-9/18:0 were analyzed in total lipids extracted from liver (G) and C4-2 tumor (H) tissues. Columns, mean; bars, SE. *, $P < 0.05$; **, $P < 0.01$; ***, $P < 0.001$.

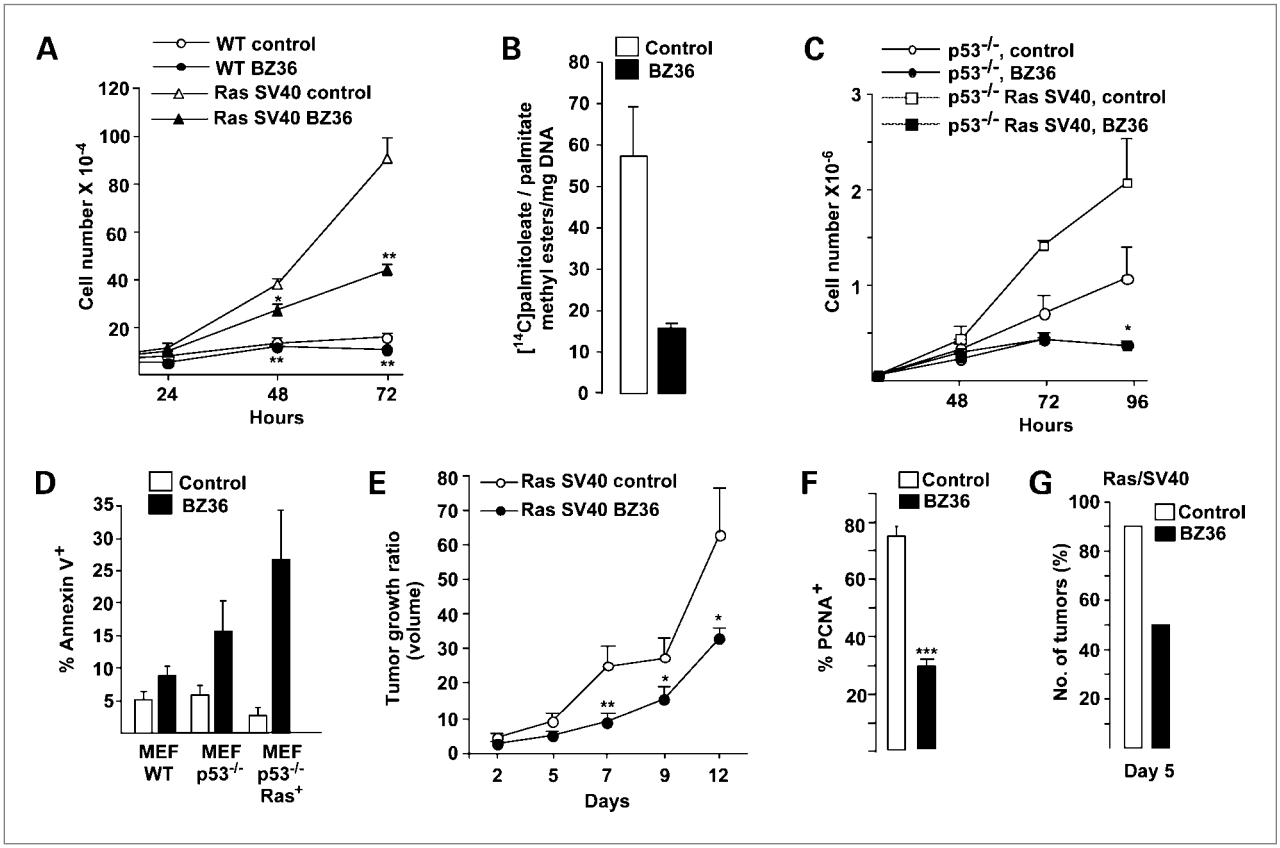


Figure 6. Inhibition of SCD1 activity restrains proliferation, increases apoptosis in Ras SV40–transformed MEFs *in vitro*, and decreases tumor growth of Ras SV40 MEF xenografts *in vivo*. A, proliferation of wild-type (WT), SV40-immortalized, or Ras SV40–transformed MEFs was measured with a hematocytometer at 24, 48, and 72 h following culture with control media or 25 μmol/L BZ36 inhibitor. B, SCD1 Δ9-desaturase activity was analyzed by measuring the conversion of exogenous $^{14}$C-saturated palmitic acid substrate into monounsaturated palmitoleic acid following exposure to control media or 25 μmol/L BZ36 inhibitor. C, proliferation of p53 knockout- or Ras-transformed p53 knockout MEFs was measured with a hematocytometer at 24, 48, and 72 h following culture with control media or 25 μmol/L BZ36 inhibitor. D, effect of the inhibition of SCD1 activity on apoptosis induction was analyzed by fluorescence-activated cell sorting by measuring the percentage of Annexin V–positive Ras SV40 MEFs at 24 h after exposure to control media or 25 μmol/L BZ36 inhibitor. E, tumor volume progression of s.c. implanted Ras SV40 MEFs in nude athymic mice was measured weekly following daily i.p. injection with BZ36 at 80 mg/kg or with vehicle. F, PCNA immunostaining of proliferative Ras SV40 MEFs s.c. implanted 14 d following daily i.p. injection with BZ36 at 80 mg/kg or with vehicle. Six fields per section were analyzed for PCNA immunostaining indicative of cell proliferation. Sections of tumors of all mice were analyzed. At least 300 cells were counted per tumor. G, the delay in tumor apparition following s.c. injection of $5 \times 10^5$ Ras SV40-tranformed MEFs was compared in mice that received daily injection of vehicle or BZ36 at 80 mg/kg during 1 wk before tumor cell injection. Columns, mean of at least two independent experiments done in triplicates; bars, SD. *, $P < 0.05$; **, $P < 0.01$; ***, $P < 0.001$.

vehicle only. This treatment significantly and reproducibly reduced the size of tumors induced in these animals all along the 12 days of this experiment (Fig. 6E). Accordingly, PCNA immunostaining on these tumors showed a significant 61% decrease in the number of proliferative cells (PCNA positive) in BZ36-treated tumors compared with vehicle-treated tumors (Fig. 6F). Strikingly, pretreatment of mice with BZ36, 1 week before injection with transformed cells, also reduced tumor formation in these animals. Indeed, 5 days after cells were grafted, almost all of vehicle-treated mice developed tumors, whereas tumors were observed in only 50% of BZ36-treated mice (Fig. 6G). Collectively, these data confirmed our observation with LNCaP and C4-2 human cancer cell lines and show that inhibition of SCD activity has a potent inhibitory effect on the cell viability and tumorigenicity of p53-deficient and Ras-transformed cells.

## Discussion

Many efforts have been directed during the last years toward more efficient ways to ablate pathways implicated in signaling from growth receptors in cancer cells. These new kinase-directed therapies have been of some success in several cancers, whereas still long lists of cancers, including prostate cancer, are unfortunately refractory to these treatments. Although dramatic metabolic differences have been described from long time ago between normal and cancer cells, little efforts have been invested in targeting metabolic pathways for the treatment of cancer. We have previously shown a close relationship between metabolic responses and proliferative stimuli (21–23). Changes in this coordinated response might lead to abnormal metabolic changes during tumor development and cancer progression. In the present study, we

show that targeting SCD1, a key lipogenic enzyme required for the biosynthesis of MUFA, might be of great benefit for the treatment of prostate cancer.

One important finding in our study is the increase in MUFA/SFA ratio in prostate cancer tissue from patients with Gleason ≥7, compared with patients with benign prostatic hyperplasia, and in particular the increase of the monounsaturated palmitoleate and oleate, which are the major products of SCD1. Consistent with this observation, we show for the first time the overexpression of SCD1 in human prostate cancer tissues as well as androgen-sensitive and androgen-resistant prostate cancer cell lines. We thus have analyzed the effects of SCD1 inhibition in prostate cancer cells and prostate tumor xenografts in mice, and we have dissected the molecular mechanisms underlying these effects. Inhibition of MUFA synthesis through inactivation of SCD1 enzymatic activity results in major changes in complex lipid composition of the cell, decreases cell proliferation, abrogates growth of prostate tumor xenografts in mice, and significantly increases tumor-bearing mice survival. Importantly, we show that SCD1 inhibition represses proliferation of both androgen-sensitive LNCaP and androgen-resistant C4-2 prostate cancer cells *in vitro* and *in vivo*, suggesting that it may represent a potent target during the progression of prostate cancer toward an androgen-independent status. Interestingly, it has been previously noticed that although FAS expression in prostate cancer is initially sensitive to androgens, this sensitivity is lost in parallel with the emergence of the androgen-independent phenotype (24, 25). Furthermore, the changes in lipid synthesis following SCD1 repression are translated into the inhibition of the AKT pathway, which is certainly one of the major signaling pathways implicated in advanced prostate cancer (26–28). Indeed, oncogenic signaling converges in the AKT pathway (29), and this pathway functions to promote tumor growth and the emergence of hormone-refractory disease (30, 31). SCD1 actively participates in the generation of phosphatidylinositols, which are precursors of PI(3,4,5)$P_3$, a known AKT activator. Consistent with this role of SCD1, we found decreased concentration of PI(3,4,5)$P_3$ in prostate cancer cells treated with BZ36, concomitant with a decrease in AKT phosphorylation. Furthermore, targeting AKT pathway results in the inhibition of prostate tumors in mice (27). On the other hand, AKT activation is important for triggering the metabolic switch in cancer cells. First, regulating hexokinase and ATP citrate lyase activity results in increased lipid synthesis substrates. Hexokinase accelerates glycolysis, resulting in increased formation of citrate, which is catalyzed to acetyl-CoA in the cytoplasm for lipid synthesis (32, 33). Second, AKT stimulates the transcriptional activity of SREBP, finally resulting in increased mRNA expression of key enzymes for lipid synthesis, such as FAS or SCD1 (34, 35). Our results strongly suggest that SCD1 inhibition creates a negative loop in which AKT inactivation results not only in decreased proliferation and apoptosis of cancer cells but also in decreased lipid synthesis. Inhibition of *de novo* FA synthesis may also overcome inactivation of *PTEN*, which is frequently mutated in prostate cancer (36). Because PTEN inactivates AKT by degrading PI(3,4,5)$P_3$, the PTEN inactivation found in cancers shows that elevated PI(3,4,5)$P_3$ levels contribute to oncogenesis (37). Because PTEN is not expressed in prostate cancer LNCaP and C4-2 cells, our study could be also representative of prostate tumors that carry mutations in *PTEN* (36). Interestingly, PNT2 cells express functional PTEN protein, and SCD1 inhibitor does almost not affect proliferation of these cells, which suggest that the effects of this treatment are mediated by decreased production of PI(3,4,5)$P_3$. This is further supported by our observation that prostate cancer cell proliferation potential and AKT signaling were rescued from the repressive effect of SCD1 inhibitor following addition of external PI(3,4,5)$P_3$.

AKT also inhibits GSK3α/β (38). We found that GSK3α/β is activated following SCD1 inhibition, likely through AKT pathway abrogation (Fig. 4C). Consistent with this finding are the decrease in β-catenin activity (Fig. 4F) and the general decrease in the β-catenin growth-promoting transcriptional targets (Fig. 4G). Complementary to this finding is the observed activation of the AMPK pathway. It has been previously shown that oncogenic signaling impairs AMPK activation through LKB1 inhibition (39). Conversely, AMPK activation inhibits prostate cancer cell proliferation (40), although the precise mechanism whereby AMPK activation induces growth arrest in cancer cells is complex. Several pathways are likely implicated, including p53, p21, or p27 (41, 42). Our results further support that AMPK activation may interfere with cancer cell metabolism, at least in large part, through the AKT pathway. About the energy status of the cell, the AMP/ATP ratio is expected to be low in cancer cells, a condition in which AMPK is inactive. As a result of lipid synthesis inhibition and AKT pathway abrogation, AMPK may become active. Activated AMPK inhibits on its turn the AKT target and activator mammalian target of rapamycin through both TSC1-2 activation (43) and direct AKT inhibition (40). In addition, AMPK also inhibits lipid synthesis pathways, which are essential for AKT activation (44). Summarizing, AMPK activation results in a concomitant inhibition of AKT pathway.

Finally, we show that cell transformation by oncogenic signaling, such as Ras-mediated tumorigenesis, requires intact lipid synthesis pathways because inhibition of lipogenesis, such as observed when SCD1 inhibitor is used, prevents Ras-mediated transformation and significantly delays Ras-mediated tumorigenesis of primary fibroblastic cells (Fig. 6). This finding strongly suggests that oncogenic signaling triggers a metabolic response that directs the cell to particular lipid synthesis pathways that will facilitate cancer cell growth and survival. Interestingly, in addition to modification of growth factor receptor systems in the cellular membrane, and generating signaling lipids, this modification in lipid synthesis modulates

on its turn the activation of Ras and other oncogenic pathways through protein lipidation, such as *N*-myristoylation and *S*-palmitoylation (45). Strikingly, it was recently reported that some Wnt proteins are modified by palmitoleate, which is the direct product of SCD1 activity, and that this modification is required for secretion and/or signaling activities of secreted signaling proteins, such as the Wingless proteins Wnt-1 and Wnt-3a (46). This creates a positive feedback loop that contributes to sustained cancer cell growth and proliferation. Interesting for our study, although *Ras* mutations are rare in prostate cancer, activation of the Ras pathway is a common feature of this cancer (47, 48). Moreover, it has been shown that in prostate cancer a cooperative Ras and Wnt oncogenic signaling exists (49). Indeed, our finding that SCD1 activity is required for Ras-mediated tumorigenesis in MEFs may be of great importance for understanding oncogenic signaling in prostate cancer and may support further investigations.

Treatment of prostate cancer is a major goal to be achieved, and we believe that SCD1 targeting should be considered as an alternative or complementary treatment of prostate cancer. Perhaps, the most important finding in our study is the inhibition of prostate tumor growth or even tumor remission in a mice model of prostate cancer following pharmacologic inhibition of SCD1 with the small-molecule BZ36. Consistent with our work, increased expression of SCD1 was found in lung and liver cancers (19, 50).

## Disclosure of Potential Conflicts of Interest

No potential conflicts of interest were disclosed.

## Acknowledgments

We thank Dr. L. Le Cam and members of the Fajas' lab for support and discussions and Denis Greuet for animal care.

## Grant Support

Association pour la Recherche contre le Cancer, Fondation pour la Recherche Médicale, and Institut National du Cancer.

The costs of publication of this article were defrayed in part by the payment of page charges. This article must therefore be hereby marked *advertisement* in accordance with 18 U.S.C. Section 1734 solely to indicate this fact.

Received 12/03/2009; revised 03/17/2010; accepted 04/13/2010; published OnlineFirst 06/08/2010.



## References

1. Nelson PS, Clegg N, Arnold H, et al. The program of androgen-responsive genes in neoplastic prostate epithelium. Proc Natl Acad Sci U S A 2002;18:11890–5.
2. Huggins C. Endocrine-induced regression of cancers. Science 1967; 3778:1050–4.
3. Feldman BJ, Feldman D. The development of androgen-independent prostate cancer. Nat Rev Cancer 2001;1:34–45.
4. Warburg O. Metabolism of tumors. London: Arnold Constable; 1930.
5. Warburg O. On respiratory impairment in cancer cells. Science 1956; 3215:269–70.
6. Warburg O. On the origin of cancer cells. Science 1956;3191: 309–14.
7. Vander Heiden MG, Cantley LC, Thompson CB. Understanding the Warburg effect: the metabolic requirements of cell proliferation. Science 2009;5930:1029–33.
8. Medes G, Thomas A, Weinhouse S. Metabolism of neoplastic tissue. IV. A study of lipid synthesis in neoplastic tissue slices *in vitro*. Cancer Res 1953;1:27–9.
9. Mashima T, Seimiya H, Tsuruo T. *De novo* fatty-acid synthesis and related pathways as molecular targets for cancer therapy. Br J Cancer 2009;9:1369–72.
10. Kuhajda FP. Fatty-acid synthase and human cancer: new perspectives on its role in tumor biology. Nutrition 2000;3:202–8.
11. Kuhajda FP, Jenner K, Wood FD, et al. Fatty acid synthesis: a potential selective target for antineoplastic therapy. Proc Natl Acad Sci U S A 1994;14:6379–83.
12. Nagy P, Vereb G, Sebestyen Z, et al. Lipid rafts and the local density of ErbB proteins influence the biological role of homo- and hetero-associations of ErbB2. J Cell Sci 2002;22:4251–62.
13. Menendez JA, Lupu R. Fatty acid synthase and the lipogenic phenotype in cancer pathogenesis. Nat Rev Cancer 2007;10:763–77.
14. Swinnen JV, Brusselmans K, Verhoeven G. Increased lipogenesis in cancer cells: new players, novel targets. Curr Opin Clin Nutr Metab Care 2006;4:358–65.
15. Miyazaki M, Flowers MT, Sampath H, et al. Hepatic stearoyl-CoA desaturase-1 deficiency protects mice from carbohydrate-induced adiposity and hepatic steatosis. Cell Metab 2007;6:484–96.
16. Patra SK. Dissecting lipid raft facilitated cell signaling pathways in cancer. Biochim Biophys Acta 2008;2:182–206.
17. Fu JM, Kodomuru V, Sun S, et al. Nicotinamide derivatives and their use as therapeutic agents. United States patent US 2005/0119251 A1.
18. Sarruf DA, Iankova I, Abella A, Assou S, Miard S, Fajas L. Cyclin D3 promotes adipogenesis through activation of peroxisome proliferator-activated receptor γ. Mol Cell Biol 2005;22:9985–95.
19. Scaglia N, Igal RA. Inhibition of stearoyl-CoA desaturase 1 expression in human lung adenocarcinoma cells impairs tumorigenesis. Int J Oncol 2008;4:839–50.
20. Wilson R, Sargent JR. Chain separation of monounsaturated fatty acid methyl esters by argentation thin-layer chromatography. J Chromatogr A 2001;1–2:251–7.
21. Abella A, Dubus P, Malumbres M, et al. Cdk4 promotes adipogenesis through PPARγ activation. Cell Metab 2005;4:239–49.
22. Fajas L, Egler V, Reiter R, et al. The retinoblastoma-histone deacetylase 3 complex inhibits the peroxisome proliferator-activated receptor γ and adipocyte differentiation. Dev Cell 2002:903–10.
23. Fajas L, Egler V, Reiter R, Miard S, Lefebvre AM, Auwerx J. PPARγ controls cell proliferation and apoptosis in an RB-dependent manner. Oncogene 2003;27:4186–93.
24. Pizer ES, Pflug BR, Bova GS, Han WF, Udan MS, Nelson JB. Increased fatty acid synthase as a therapeutic target in androgen-independent prostate cancer progression. Prostate 2001;2:102–10.
25. Rossi S, Graner E, Febbo P, et al. Fatty acid synthase expression defines distinct molecular signatures in prostate cancer. Mol Cancer Res 2003;10:707–15.
26. Davies MA, Koul D, Dhesi H, et al. Regulation of Akt/PKB activity, cellular growth, and apoptosis in prostate carcinoma cells by MMAC/PTEN. Cancer Res 1999;11:2551–6.
27. Kinkade CW, Castillo-Martin M, Puzio-Kuter A, et al. Targeting AKT/mTOR and ERK MAPK signaling inhibits hormone-refractory prostate cancer in a preclinical mouse model. J Clin Invest 2008;9:3051–64.
28. de Souza P, Russel P, Kearsley J. Role of the Akt pathway in prostate cancer. Curr Cancer Drug Targets 2009;2:163–75.
29. Manning BD, Cantley LC. AKT/PKB signaling: navigating downstream. Cell 2007;7:1261–74.

30. Kreisberg JI, Malik SN, Prihoda TJ, et al. Phosphorylation of Akt ($Ser^{473}$) is an excellent predictor of poor clinical outcome in prostate cancer. Cancer Res 2004;15:5232–6.
31. Shen MM, Abate-Shen C. Pten inactivation and the emergence of androgen-independent prostate cancer. Cancer Res 2007;14: 6535–8.
32. Elstrom RL, Bauer DE, Buzzai M, et al. Akt stimulates aerobic glycolysis in cancer cells. Cancer Res 2004;11:3892–9.
33. Bauer DE, Hatzivassiliou G, Zhao F, Andreadis C, Thompson CB. ATP citrate lyase is an important component of cell growth and transformation. Oncogene 2005;41:6314–22.
34. Van de Sande T, De Schrijver E, Heyns W, Verhoeven G, Swinnen JV. Role of the phosphatidylinositol 3′-kinase/PTEN/Akt kinase pathway in the overexpression of fatty acid synthase in LNCaP prostate cancer cells. Cancer Res 2002;3:642–6.
35. Bandyopadhyay S, Pai SK, Watabe M, et al. FAS expression inversely correlates with PTEN level in prostate cancer and a PI 3-kinase inhibitor synergizes with FAS siRNA to induce apoptosis. Oncogene 2005;34:5389–95.
36. Li J, Yen C, Liaw D, et al. PTEN, a putative protein tyrosine phosphatase gene mutated in human brain, breast, and prostate cancer. Science 1997;5308:1943–7.
37. Wymann MP, Schneiter R. Lipid signalling in disease. Nat Rev Mol Cell Biol 2008;2:162–76.
38. Cross DA, Alessi DR, Cohen P, Andjelkovich M, Hemmings BA. Inhibition of glycogen synthase kinase-3 by insulin mediated by protein kinase B. Nature 1995;6559:785–9.
39. Zheng B, Jeong JH, Asara JM, et al. Oncogenic B-RAF negatively regulates the tumor suppressor LKB1 to promote melanoma cell proliferation. Mol Cell 2009;2:237–47.
40. Rattan R, Giri S, Singh AK, Singh I. 5-Aminoimidazole-4-carboxamide-1-β-D-ribofuranoside inhibits cancer cell proliferation *in vitro* and *in vivo* via AMP-activated protein kinase. J Biol Chem 2005;47:39582–93.
41. Jones RG, Plas DR, Kubek S, et al. AMP-activated protein kinase induces a p53-dependent metabolic checkpoint. Mol Cell 2005;3: 283–93.
42. Hardie DG. AMP-activated/SNF1 protein kinases: conserved guardians of cellular energy. Nat Rev Mol Cell Biol 2007;10:774–85.
43. Inoki K, Ouyang H, Zhu T, et al. TSC2 integrates Wnt and energy signals via a coordinated phosphorylation by AMPK and GSK3 to regulate cell growth. Cell 2006;5:955–68.
44. Long YC, Zierath JR. AMP-activated protein kinase signaling in metabolic regulation. J Clin Invest 2006;7:1776–83.
45. Nadolski MJ, Linder ME. Protein lipidation. FEBS J 2007;20: 5202–10.
46. Takada R, Satomi Y, Kurata T, et al. Monounsaturated fatty acid modification of Wnt protein: its role in Wnt secretion. Dev Cell 2006;6:791–801.
47. Voeller HJ, Wilding G, Gelmann EP. v-rasH expression confers hormone-independent *in vitro* growth to LNCaP prostate carcinoma cells. Mol Endocrinol 1991;2:209–16.
48. Gioeli D. Signal transduction in prostate cancer progression. Clin Sci (Lond) 2005;4:293–308.
49. Pearson HB, Phesse TJ, Clarke AR. K-ras and Wnt signaling synergize to accelerate prostate tumorigenesis in the mouse. Cancer Res 2009;1:94–101.
50. Yamashita T, Honda M, Takatori H, et al. Activation of lipogenic pathway correlates with cell proliferation and poor prognosis in hepatocellular carcinoma. J Hepatol 2009;1: 100–10.